COMBUSTION SCIENCE AND TECHNOLOGY
2018, VOL. 190, NO. 8, 1455–1471
https://doi.org/10.1080/00102202.2018.1452128

Taylor & Francis
Taylor & Francis Group

Check for updates

# Experimental and numerical study of laminar flame extinction for syngas and syngas-methane blends

Weichao Wang, Ahmet E. Karatas, Clinton P. T. Groth, and Ömer L. Gülder

Institute for Aerospace Studies, University of Toronto, Toronto, Ontario, Canada

**ABSTRACT**

Extinction strain rates of syngas and syngas–methane blends at atmospheric pressure were investigated in laminar counter-flow diffusion flames as a function of nitrogen dilution through both experiment and two-dimensional axisymmetric full-domain numerical simulations. Three representative compositions of syngas were examined along with two syngas–methane blends for a range of fuel mole fractions. An opposed-jet burner configuration with straight-tube fuel and air nozzles was used in the experiments and an advanced, computational, solution algorithm was used to obtain the corresponding simulation results. Very good agreement was found between predicted and experimentally observed flame structure as well as global strain rate extinction limits for all syngas fuel and syngas–methane blends over the full range of flow rates and fuel mole fractions considered. Additionally, the local strain rate near extinction was shown to correlate with the global strain rate and an explanation of the differences between these two values was provided by the predicted changes in the nozzle exit plane velocity profiles as a function of flow rate. In particular, non-zero gradients in the axial center-line velocity were predicted at the nozzle exit plane for higher flow rates due to the pressure field created by the opposed-jet flows. The syngas extinction limits as a function of fuel composition were examined. While the amount of hydrogen was found to have a dominant effect on the extinction strain limits, methane and carbon monoxide were also found to induce early extinction and increase reactivity, respectively, if present in sufficiently large quantities.

**ARTICLE HISTORY**
Received 21 September 2017
Revised 9 January 2018
Accepted 19 January 2018

**KEY WORDS**
Biofuels; Syngas; Syngas–methane blends; Flame extinction; Extinction strain rate; Counter-flow laminar diffusion flames

## Introduction and motivation

Syngas is a biologically sourced alternative fuel that describes any gaseous mixture containing various amounts of carbon monoxide, carbon dioxide, and hydrogen as its main ingredients, but can also include other gaseous compounds in the mixture (Biofuel.org.uk, 2010). It is often produced from the gasification of a variety of different waste biomass sources such as wood, coal, and non-edible waste from food crops (Somerville et al., 2010). As a result, syngas does not have a single chemical composition and variations in composition can arise depending on the feed-stock material and method of production. Understanding the influence of composition on syngas combustion properties is therefore one of the important research concerns.

**CONTACT** Clinton P. T. Groth groth@utias.utoronto.ca; Ömer. L. Gülder ogulder@utias.utoronto.ca University of Toronto Institute for Aerospace Studies, Toronto, Ontario, Canada

Color versions of one or more of the figures in the article can be found online at www.tandfonline.com/gcst.

© 2018 Taylor & Francis

An important combustion characteristic for diffusion flames is the extinction strain rate (Williams, 2001). It is a measure of fuel flammability and the susceptibility of flames to suppression. There has been a limited number of studies conducted on the extinction limits of syngas and, of those, the numerical components have been largely based on now standard one-dimensional (1D) numerical analyses (Ding et al., 2011; Park et al., 2009; Shih and Hsu, 2011; Som et al., 2008). The present study considers a combined experimental and numerical effort to examine extinction strain in laminar counter-flow (opposed-jet) diffusion flames for a range of syngas and syngas–methane blends. Furthermore, the numerical analysis of extinction was conducted using an advanced computational solution procedure on two-dimensional (2D) axisymmetric domains allowing greater insight into the extinction behavior than that afforded by conventional 1D analyses.

The syngas fuel compositions and syngas–methane blends considered herein are listed in Table 1 with their respective compositions, in terms of mole fraction. The S1, S2, and S5 syngas fuels were selected to be representative of typical syngas compositions and include variation in the hydrogen/carbon monoxide ratio and methane level. The S5M25 and S5M50 fuels are syngas–methane blends, where the syngas S5 is blended with 25% and 50% methane by mole fraction (or volume), respectively, as indicated in the table.

## Counter-flow burner and experimental methodology

Strain rate is representative of the residence time of reactants in the reaction zone and small aerodynamic time scales are indicative of elevated strain rates. In a counter-flow laminar diffusion flame, the aerodynamic strain rate is defined in terms of the gradient of the axial velocity component, $\partial U/\partial x$, where $U$ is the axial component of velocity and $x$ is the position coordinate in the axial direction along the burner center line. The convention within literature is to express the local strain rate, $a_l$, as

$$a_l = \left.\frac{\partial U}{\partial x}\right|_{\max} \tag{1}$$

just prior to the thermal mixing layer of the flame on either the air or fuel side, depending on the location of the flame with respect to the stagnation plane (Egolfopoulos et al., 1989; Sarnacki et al., 2012; Yu et al., 1986). The stoichiometric mixture fraction, $Z_{st}$ (Du and Axelbaum, 1995), which can be used to position the flame with respect to the stagnation plane in $Z$ (mixture fraction) space is given as (Xia and Axelbaum, 2013)

$$Z_{st} = \left(1 + \frac{Y_R W_O \nu_O}{Y_O W_R \nu_R}\right)^{-1} \tag{2}$$

**Table 1.** Syngas compositions and syngas–methane blends.

| | Fuel designation | $H_2$/CO | $X_{CO}$ | $X_{H_2}$ | $X_{CO_2}$ | $X_{CH_4}$ |
|---|---|---|---|---|---|---|
| Syngas compositions | S1 | 0.5 | 0.50 | 0.25 | 0.25 | 0 |
| | S2 | 1.0 | 0.375 | 0.375 | 0.25 | 0 |
| | S5 | 1.0 | 0.375 | 0.375 | 0.20 | 0.05 |
| Syngas–methane blends | S5M25 | 1.0 | 0.28125 | 0.28125 | 0.15 | 0.2875 |
| | S5M50 | 1.0 | 0.1875 | 0.1875 | 0.10 | 0.525 |

where $Y$, $W$, and $\nu$ are mass fractions, molecular weight, and stoichiometric coefficient, respectively, and the subscripts $_R$ and $_O$ denote the reactant and oxidizer chemical species in fuel and air streams, respectively. The stagnation plane is located at $Z_{st} = 0.50$, and thus flames located on the air and fuel side of the stagnation plane have values of $Z_{st} < 0.50$ and $Z_{st} > 0.50$, respectively.

In the absence of direct measures of $a_l$, the local strain rate can be approximated by the global strain rate as first formulated by Seshadri and Williams (1978), which is a function of nozzle exit bulk flow velocities, nozzle separation, and the densities of fuel and air streams. Potential flow is assumed within the counter-flow geometry which predicts a linear deceleration of the axial component of velocity as the gases approach the stagnation plane. Factoring in a correction for the density differences of the fuel and air streams, the global strain rate, $a_g$, can be expressed as

$$a_g = \frac{2V_A}{L}\left[1 + \frac{V_F}{V_A}\left(\frac{\rho_F}{\rho_A}\right)^{1/2}\right] \tag{3}$$

where $L$, $V$, and $\rho$ denote nozzle separation distance, nozzle bulk flow velocity, and density, respectively, and the subscripts $_F$ and $_A$ denote fuel and air streams, respectively.

The experimental apparatus used herein consists of a single counter-flow burner, designed specifically to handle high flow conditions (Wang, 2014). The burner includes two identical nozzle assemblies, each with inner and concentric nozzles. See Figure 1. The inner nozzles supply the fuel mixture (fuel diluted with nitrogen) and air streams from the lower and upper assemblies, respectively, while the outer nozzles of both assemblies supply co-flow nitrogen, which isolates the flame from the ambient atmosphere. Two interchangeable inner nozzle configurations are available for the counter-flow burner. One configuration of the inner nozzle (parabolic profile configuration as depicted on right side of figure) has smooth bore tubes, for which a parabolic velocity distributions are expected at the nozzle exits in accordance with laminar pipe flow theory. However, as will be shown, in reality the parabolic configuration may result in somewhat different inflow conditions at the nozzle exit plane that are subject to variations depending on the pressure field generated by the opposed jets. The second configuration (uniform profile configuration as depicted on left side of figure) incorporates a sintered metal matrix 5.1 mm upstream of the nozzle exit plane, with the intention of creating uniform or top-hat velocity profiles at the nozzle exit planes. As will also be shown, the matrix is however not sufficient to ensure idealized uniform profiles of fuel and air at the nozzle exits. Similar sintered metal matrix meshes are fitted in the outer nozzles used to supply the co-flow nitrogen so as to provide similar uniform inflow velocity profiles in both burner configurations. The radii of the inner nozzles are 5.6 mm and 5.1 mm and tube wall thicknesses are 0.76 mm and 1.27 mm, respectively, for the so-called parabolic and uniform profile configurations. The nozzle separation distance, $L$, was maintained at 10.2 mm, such that the burner $L/D$ ratio was either 0.91 or 1, depending on the configuration of the inner nozzles, where $D$ represents the inner nozzle diameter. The radius and tube wall thickness of the

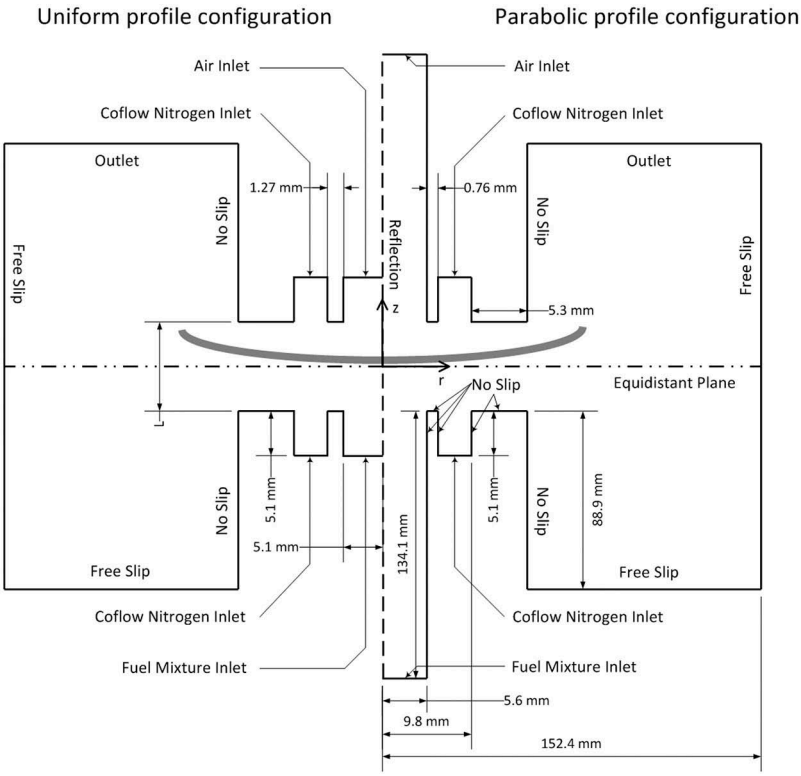


**Figure 1.** Schematic diagram (not to scale) of 2D axisymmetric counter-flow burner and computational domain and boundary conditions used in numerical simulations showing both uniform (left) and parabolic (right) profile configurations (identical dimensions in both configurations are labeled only on the right).

outer nozzle are 9.8 mm and 5.3 mm, respectively. A ceramic glass enclosure houses the burner, allowing visual and optical access to the flame. A chimney system located on the top of the burner ensures that the exhaust is properly vented from the laboratory.

The strain rate in the experiments was controlled by adjusting the flow rates of fuel mixture and air streams using flow controllers with calibrated accuracy within 1%. A stable flame was first established near but below the extinction limit and the experiments were then carried out by gradually applying small or incremental increases to the flow strain rate, through sequential increases to the bulk mass flow rates of the fuel, dilution nitrogen, and air streams, respectively, until the flames were extinguished. At each step of this process, a constant fuel mole fraction and momentum balance of the fuel mixture and air streams were maintained. Additionally, the flame was monitored and allowed about 30 s to stabilize between each step. Each step change in strain rate was maintained at about 1–5% of the global extinction strain rate and the experiments were repeated 3–4 times for each fuel mixture. In this way, the extinction limits were accurately established.

## Numerical simulation of counter-flow burner and flame extinction

### *Finite-volume solution method*

The computational framework developed by Charest et al. (2010) for the prediction of laminar reactive flows with complex chemistry, non-gray radiative heat transfer, and soot was applied to the prediction of the counter-flow diffusion flames of interest herein. This numerical modeling tool was specifically developed for use with large multi-processor parallel computers and its capabilities have been previously demonstrated in a number of recent studies of laminar co-flow diffusion flames under both high pressure and low gravity conditions (Charest et al., 2010, 2011a; 2011b; Charest et al., 2011).

The framework solves the conservation equations for a multi-component, compressible, reactive, gaseous mixture. Soot formation/oxidation and radiation were not included here since these effects are expected to be small for the syngas fuels and atmospheric pressures of interest. The governing equations are solved using a finite-volume method previously developed by Groth and co-workers (Charest et al., 2010; Gao and Groth, 2006; Gao et al., 2011; Sachdev et al., 2005). The scheme makes use of piece-wise limited linear reconstruction and an approximate Riemann solver to determine numerical values of the inviscid fluxes (Roe, 1981) and second-order diamond-path method for the viscous fluxes. Low-Mach-number preconditioning is applied to reduce the excessive dissipation and numerical stiffness of the discretized system and permit accurate solution for the low-speed flames of interest (Weiss and Smith, 1995). The solution of the fully coupled non-linear equations resulting from the finite-volume discretization procedure is relaxed to steady-state using a parallel implicit algorithm which uses a matrix-free Newton–Krylov method. Thermodynamic/transport properties and gas-phase reaction rates are evaluated using CANTERA (Goodwin, 2003).

The simulations were performed using a reduced mechanism consisting of 19 species and 86 reactions by Slavinskaya et al. (2008), based on the GRI-Mech 3.0 mechanism for methane combustion (Smith et al., 2000). This mechanism was specifically tuned for the combustion of methane and syngas compositions with significant hydrogen and carbon monoxide content. For the prediction of laminar flame speed and adiabatic flame temperature associated with unstrained planar 1D laminar premixed flames of syngas $H_2$/CO compositions, the reduced mechanism of Slavinskaya et al. was found to provide more agreeable results with existing experimental data than GRI-Mech 3.0. Furthermore, both Wang (2014) and Sarnacki et al. (2012) have found that the reduced mechanism provides superior predictions of extinction strain rates in laminar counter-flow diffusion flames compared to those provided by GRI-Mech 3.0.

### *Axisymmetric computational domain and grids*

The parabolic profile configuration created some uncertainty regarding the specification of the inflow velocity at the nozzle exit planes of the inner nozzles. It was found that applying idealized parabolic velocity distributions at the inflow boundaries near the nozzle exits produced poor predictions of extinction strain, particularly at high flow rates (Wang, 2014). Furthermore, the experimental study of Vagelopoulos and Egolfopoulos (1998) has shown that the nozzle velocity flow distribution is affected by the radial pressure gradient created by the opposed jets and Sarnacki et al. (2012) later demonstrated in their experiments that the nozzle velocity flow distribution deviates from a parabolic profile as the strain rate is increased. Amantini et al. (2007) approached this problem by using the measured nozzle flow distribution as the

numerical inflow boundary conditions at the nozzle exit plane. However, this approach is heavily dependent on availability of experimental data which were not available here. To overcome this issue in the present study, a full 2D axisymmetric computational domain was used. The computational domain of the inner nozzles was extended upstream by 12 times their diameter and uniform inflow velocity distributions were imposed at these upstream boundaries. By including the additional upstream portions of the inner fuel and air stream nozzles within the computational domain for the parabolic configuration, the nozzle exit plane velocity distributions were computed directly as part of the simulation such that the predicted profiles match the pressure and flow conditions at the nozzle exits.

Conversely, the uniform profile configuration was modeled by simply applying uniform inflow velocity profiles at the locations of the sintered metal matrix within the nozzles just upstream of the exit plane. Note that it was found that the sintered metal matrix was unable to maintain ideal uniform profiles at the exit planes of the inner nozzles (Wang, 2014), leading to generally poor agreement between numerical and experimental flow fields for elevated flow rates. Such an inflow condition represents the limit of the modeling capabilities here without recourse to additional information regarding the velocity profiles emerging from the metal matrix meshes.

The computational domains adopted here are shown schematically in Figure 1 for both the parabolic and uniform profile configurations. The domain in each case is symmetrical along the equidistant plane and extends 152.4 mm radially. The nozzle radii, separation distance, tube thicknesses, and far-field domain boundaries are modeled precisely based on the burner geometry and exhaust enclosure of the experimental facility. The inner nozzles extend 134.1 mm and 5.1 mm upstream from nozzle exit plane for the parabolic and uniform configurations, respectively, while the outer nozzles extend just 5.1 mm upstream to the position of the sintered metal matrix. No-slip boundary conditions were applied at the nozzle tube walls while the far-field and lower boundaries of the domain were treated as free-slip boundaries. All tube walls were taken to have a fixed temperature of 300 K. The upper boundary of the domain serves as the flow outlet, where values of temperature, velocity, and species mass fraction were extrapolated from the interior of the domain while the pressure was specified and held at a fixed value. The compositions of the gaseous mixtures were specified at all inlet boundaries, along with the velocity and temperature, while the pressure was extrapolated from the interior of the domain. Uniform velocity and temperature profiles were specified for the air, fuel mixture, and co-flow nitrogen inlet boundaries, in all cases.

For the parabolic profile configuration, the computational mesh was subdivided into 180 cells and 18 blocks in the radial and 672 cells and 42 blocks in the axial directions, respectively. The resulting structured but non-uniformly-spaced mesh consisted of 92,160 quadrilateral cells within 576 blocks. For the uniform profile configuration, the computational mesh was subdivided into 180 cells and 18 blocks in the radial and 640 cells and 40 blocks in the axial direction. This produced a mesh consisting of 81,920 cells and 512 blocks. In both cases, the cells were clustered radially toward the center line and axially toward the equidistant plane so as to provide higher resolution for regions containing the flow. The vertical mesh spacing between the inner nozzles was approximately 35 $\mu$m, while the spacing was approximately 140 $\mu$m in the radial direction. The computational grid used in the simulations of the parabolic profile burner configuration is depicted in Figure 2, showing the distribution of both the grid blocks and quadrilateral cells. The

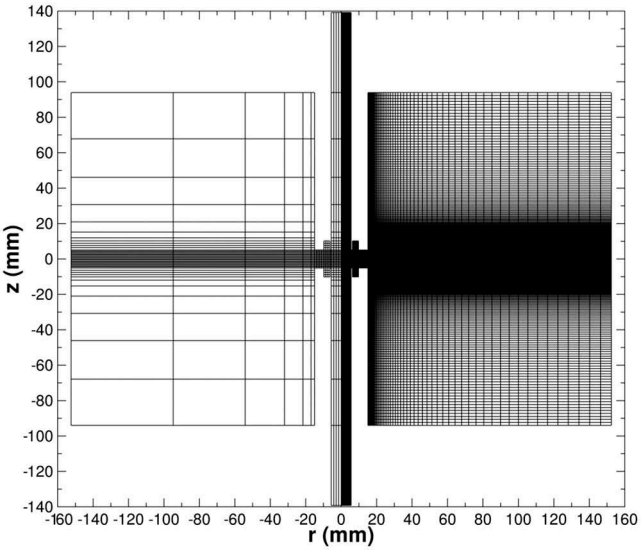


**Figure 2.** Computational mesh used in 2D axisymmetric simulations of the counter-flow burner for parabolic profile configuration showing the computational blocks of the multi-block grid (left) as well as the distribution of the computational cells (right); grid consists of 576 blocks and 92,160 quadrilateral cells.

mesh used for the simulation of the uniform profile burner was very similar. A systematic mesh refinement study was performed to ensure that the resolutions of these two meshes were sufficient for the purposes of the present extinction studies (Wang, 2014).

### *Procedure for computation of extinction limits*

Numerical extinction was determined in a manner similar to that adopted in the experiments. A converged steady counter-flow flame solution was first established well below the expected extinction strain limit. The converged solution was then used as an initial estimate or starting solution for determining a new solution at a higher strain rate, with the higher strain rate imposed by simply modifying the inflow boundary conditions and prescribing higher bulk flow velocities in the fuel and air stream nozzles. This process was repeated in an iterative manner until the numerical solution no longer supported a flame and a precise value for the extinction strain rate was established. The final step size increases in the global strain rate at extinction were kept sufficiently small, as summarized in Table 2, to ensure that the error in the computed extinction strain rate was below 3%.

## Analyses and comparison of experimental and numerical results

### *Observed flame structure*

To illustrate the quality of the present numerical simulations, a visual comparison between an experimental image of the burner and counter-flow flame to 2D numerical predictions of the flame structure is provided in Figure 3 for a pure syngas S1-air flame at $a_g = 600\ s^{-1}$.

**Table 2.** Strain rate step sizes used in the computation of the flame extinction limit.

| $a_g$ ($s^{-1}$) | $\leq 200$ | $\leq 500$ | $\leq 1000$ | $\geq 1001$ |
|---|---|---|---|---|
| Step size ($s^{-1}$) | 2 | 5 | 10 | 20 |

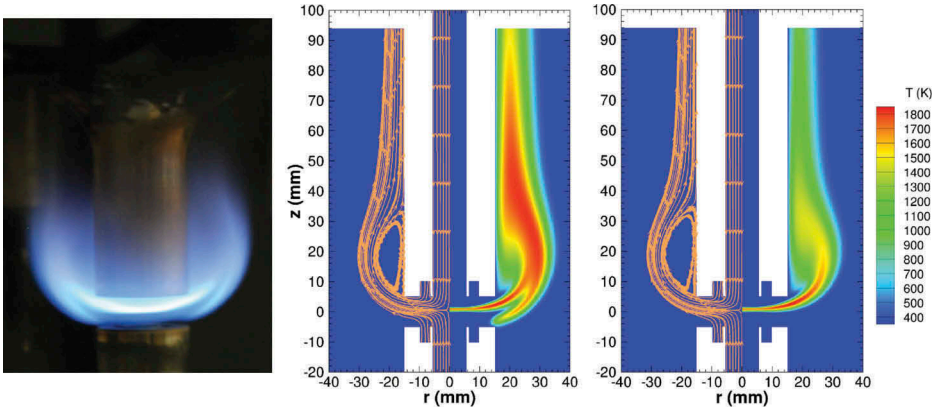


(a) Experimental image of burner and flame.

(b) Numerical prediction with air in outer domain.

(c) Numerical prediction with $N_2$ in outer domain.

**Figure 3.** Qualitative comparison of flame structure for pure syngas S1-air counter-flow diffusion flame at $a_g = 600\ s^{-1}$ comparing (a) experimental image of flame and burner to numerical predictions of flame with (b) air and (c) nitrogen-initialized domains for parabolic burner configuration.

The predicted extent of the inner flame disk structure can be seen to be in rather good agreement with the experimental image. The presence of the unwanted outer flame in experiments, due to excess fuel reacting with oxygen, was eliminated in the numerical solutions by initializing the outer domain with pure nitrogen in place of air and was shown not to effect the computed inner flame structure and extinction limits as indicated in the figure (Wang, 2014). Additionally, although the computed outer flame for the air case is not needed in the current study, it seems to be captured reasonably well by the finite-volume method.

At this point, a number of comments can also be made regarding the observed structures of the experimental and numerical flames for the fuels investigated. The flame disk structure was found to increase in size and become thinner as the strain rate was increased. Furthermore, the maximum flame temperature in the numerical solutions was found to be higher as the fuel mole fraction was increased, due to the increased concentrations of more reactants. The flames for all of the syngas compositions and syngas–methane blends were also observed to be blue in color during the experiments, indicating very little or no soot formation. Additionally, the fuels with higher hydrogen content were seen to have slightly larger flame disks for a given flow rate and fuel mole fraction than those with lower hydrogen content. This is likely due to the high diffusivity of hydrogen.

## *Global strain rate*

Experimentally measured and numerically predicted values of the global strain rates at flame extinction, $(a_g)_e$, were examined as a function of fuel mole fraction for the syngas

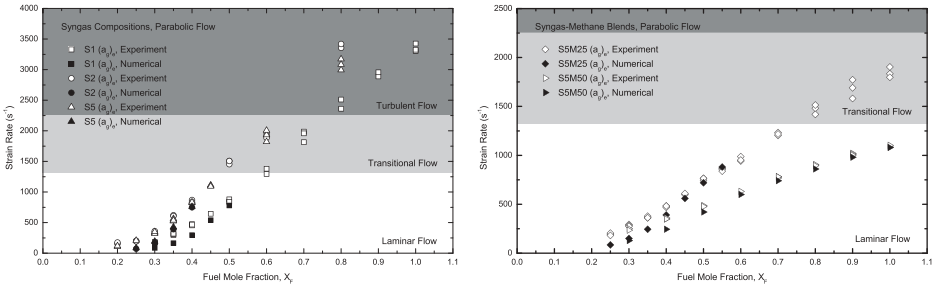


(a) Syngas compositions S1, S2, and S5. (b) Syngas-methane blends S5M25 and S5M50X.

**Figure 4.** Comparison of experimental (white symbol) and numerical (black symbol) values of the global extinction strain rates for (a) three syngas compositions and (b) two syngas–methane blends for the parabolic profile burner configuration only.

compositions and syngas–methane blends of Table 1. The results for the parabolic inflow burner configuration are presented in Figure 4 for both all of the syngas compositions as well as all syngas–methane blends. Due to the higher global strain rate extinction limits exhibited by uniform inflow configuration compared to the parabolic inflow setup, results were obtained only for S1 and S5M50, representing the syngas composition and syngas–methane blend with the lowest global extinction strain rate. The measured and predicted values of the global extinction strain rate for these cases are compared in Figure 5.

It is evident from the figures that the syngas compositions and syngas–methane blends have elevated extinction limits, especially at high fuel mole fractions, and often lie well beyond the traditional laminar regime as defined by that for pipe flow. Assuming that fully developed laminar pipe flow can be found for Reynolds number of Re $\lesssim$ 2300, turbulent pipe flow exists for Re $\gtrsim$ 4000, and that a transitional regime is present between these two values, the approximate range of the laminar, transitional, and turbulent flow regimes are indicated in Figures 4 and 5 as a function of strain rate for the present burner geometry. For all cases investigated in this study, the kinematic viscosity of air was consistently less than that of the fuel (for all compositions and blends), leading to higher Reynolds number in the air stream than the fuel stream and causing it to be the limiting stream for the onset

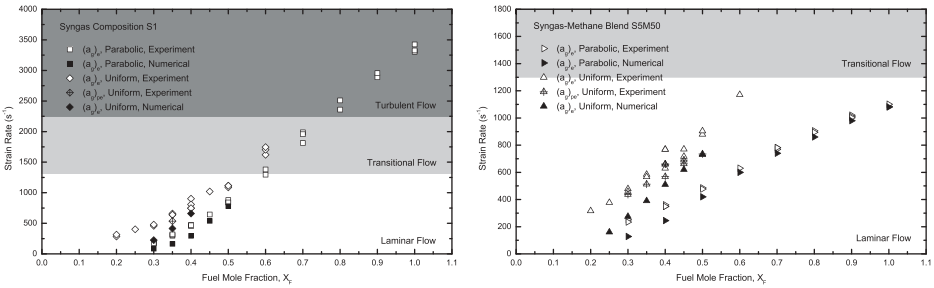


(a) Syngas composition S1. (b) Syngas-methane blend S5M50.

**Figure 5.** Comparison of experimental (white symbol) and numerical (black symbol) values of the global extinction strain rates for (a) syngas composition S1 and (b) syngas–methane blend S5M50 for both parabolic and uniform profile burner configurations.

of transitional and subsequently fully turbulent flow. Furthermore, it is noted that it was not possible to obtain numerical solutions at high flow rates in the transitional and turbulent flow regimes (i.e., for $a_g \gtrsim 1000\ s^{-1}$) due to non-steady behavior of the solutions downstream of the opposed nozzles (Wang, 2014).

It can be seen that the measured global extinction strain rates increase as the fuel mole fraction increases for all fuels investigated. The experimental data exhibit an overall trend that is approximately linear at higher fuel mole fractions for all cases; however, for syngas compositions at low fuel mole fractions, the trend deviates from this linear behavior. While there is a high degree of scattering in some of the experimental data at elevated flow rates due to unsteady flow behavior in the transitional and turbulent flow regimes, the linear trend in the experimental results seems to be maintained, even for what may be turbulent flow conditions.

The predicted global extinction strain rates show a high degree of agreement with experiment for the parabolic inflow configuration. The non-linear deviation observed in syngas compositions at low fuel mole fractions is well captured, as are the overall trends for all fuel compositions and blends below $a_g \gtrsim 1000\ s^{-1}$. The numerical results generally under-predict the experimental extinction limits at low fuel mole fractions and low flow rates, but the prediction improves as the flow rates increase. This is likely caused by the deviation of experimental flow field at low flow rates from the ideal as was observed in a previous study of methane-air (Wang, 2014). This deviation can result in higher estimates for the global strain rate in the experiments for a given local extinction rate and, consequently, lead to the present differences between the experimental and numerical results.

The experiments for the uniform inflow configuration were much less repeatable than that for the parabolic inflow cases. Additionally, the occurrences of partial flame extinctions, as indicated by the measured values, $(a_g)_{pe}$, were also common within the higher flow regimes. During these partial extinctions, a portion of the previously symmetric flame disk would extinguish abruptly, and the final extinction of the remaining flame would often occur at a significantly higher strain rate than the value for the partial extinction. The axisymmetric numerical simulations were obviously not able to capture such processes. It is believed that the existence of the partial extinctions is caused by the inability of the sintered metal matrix to maintain an ideal uniform flow profile above a certain flow rate, leading to asymmetrical flow (Wang, 2014).

The numerical predictions of global strain rate at extinction for the uniform inflow configuration agree less well with the experimentally measured values compared to those for the parabolic cases. Although the positive correlation between the extinction strain rate and fuel mole fraction is rather well captured, there is noticeable under-prediction of the extinction strain. This under-prediction of the strain rate is again believed to be caused by the deviation in the experiments from the ideal uniform inflow distribution that is explicitly imposed in the simulations due to the limitations of the sintered metal matrix. Despite these issues, it would seem that the numerical simulations were able to capture the essential differences between the two inflow burner configurations across a range of flow conditions and for several fuel compositions and blends. In particular, the global extinction strain rate for the uniform inflow configuration is greater in both the experimental and numerical results than those seen for the parabolic inflow profile.

Moreover, the differences in extinction strain rates between the two configurations become less pronounced at elevated strain rates. The latter is due to changes in the actual nozzle inflow velocity profiles as will be shown.

### *Fuel composition and extinction limits*

Extinction limits can be heavily dependent on the level of hydrogen present in the fuel because of its high diffusivity. In particular, Pellett et al. (1998) report that the extinction strain rate of pure hydrogen is up to 30 times higher than that of pure methane. In order to explore the fuel composition effects on the syngas extinction limits, the experimentally measured values of the global extinction strain rate for all syngas fuel compositions and blends investigated in the current study are re-summarized in Figure 6 for the parabolic inflow nozzle configuration only as a function of the fuel mole fraction. Additional results for methane-air counter-flow flames obtained using the same experimental setup are also shown for comparison (Wang, 2014). The numerical predictions are not shown as they are very similar and do not add to the discussion. It can be seen from the figure that pure syngas compositions have higher extinction strain rates than the syngas–methane blends, which in turn have higher extinction strain rates than pure methane. This behavior is directly correlated with the hydrogen composition within each fuel as would be expected. Higher hydrogen content results in higher global strain rates at extinction.

While the general trends in extinction for the various syngas fuels can be explained through hydrogen composition, there are several interesting exceptions to this behavior in the results. Consider, for example, the results for compositions S2 and S5. Both have identical hydrogen mole fractions of 37.5% and otherwise have the same composition except that S5 has 5% methane in place of the carbon dioxide that is present in S2. S2 and S5 exhibit similar extinction trends and both have the highest extinction strain rates of all syngas compositions and blends investigated, due to their high hydrogen content. However, at high strain rates, S2 appears to have a higher extinction strain rate than S5. Compare also the results for the syngas composition S1 and the syngas–methane blend S5M25, which have 25% and 28.125% hydrogen by volume, respectively. Curiously, S1 has

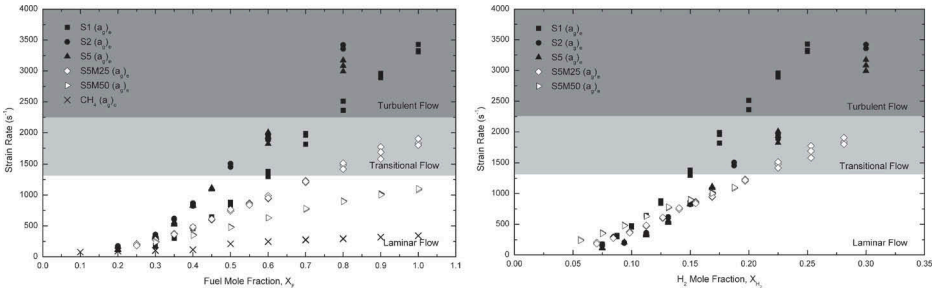


(a) Dependence of extinction strain rate on fuel mole fraction. (b) Dependence of extinction strain rate on $H_2$ mole fraction.

**Figure 6.** Comparison of measured values of the global extinction strain rates obtained using the parabolic burner configuration for all syngas compositions (black symbol), syngas–methane blends (white symbol) and methane ( $\times$ symbol) as a function of both the fuel mole fraction (a) and fuel $H_2$ mole fraction (b).

a much higher extinction strain rate than that of S5M25 at higher fuel mole fractions. The primary difference between these two fuels is that S5M25 has a higher composition of methane than S1, for which the methane is replaced by CO and $CO_2$.

To further investigate this behavior, consider the plot of measured values of the global extinction strain rate as a function of hydrogen content shown in Figure 6. If hydrogen concentrations were the only factor affecting the extinction limits, one should expect the experimental data to collapse on to a single line resembling that of the extinction behavior for pure hydrogen. However, this does not occur. Instead, the data collapses loosely into two groups: one for the syngas compositions with little or no methane and the other for syngas–methane blends that have significant methane content. At constant hydrogen concentrations, the extinction strain rates of the syngas fuels with significant methane concentration are much lower at high flow rates and fuel mole fractions. However, at the lower flow rates and fuel mole fractions, the opposite is true. These trends can be explained through the observations of Thiessen et al. (2010) and Fleck et al. (2013), where it was found that increasing the relative concentration of methane in hydrogen mixtures leads to reduced radical production, as the methane chain branching reactions consume increasingly more of the available radicals, especially OH. The results of Figure 6 also show the extinction behavior of the three syngas compositions form two separate curves: one for S1 and the other for S2 and S5. The S1 composition has significantly higher carbon monoxide and carbon dioxide content compared to the S2 and S5 compositions for a given hydrogen mole fraction. It is well documented in the literature (Herzler and Naumann, 2008; Kéromnès et al., 2013; Mittal et al., 2007) that the reactivity of syngas mixtures is dominated by hydrogen chemistry for CO concentrations lower than 50%. Hence, higher global strain rates at extinction are found for S1 as compared to the other two compositions.

## Local strain rate

With the current experimental setup, it was not possible to directly measure the local strain rate as defined by Eq. (1); however, the predicted values from the numerical simulations are investigated here and compared to the corresponding predictions of the global extinction strain rates. While the global strain rate at extinction can be defined using Eq. (3) for the flow conditions under which flame extinction occurs, the local extinction strain rate must be evaluated just prior to extinction, when the flame is still present. This is because the existence of the flame distorts and alters the velocity field. It is therefore desirable to determine the local strain rate as close to extinction as possible, in order to fairly compare local and global values of the extinction strain rates. For the majority of fuels considered herein, $Z_{st} > 0.50$. Accordingly, the local strain rates were evaluated on the fuel mixture side of the flame. On the other hand, for all syngas–methane blends, $Z_{st} < 0.50$, regardless of the dilution with nitrogen. Thus, the local strain rates in these cases were evaluated on the air side of the flame. In each case, the local strain rates, $(a_l)_{ne}$, near extinction were evaluated numerically using the flame solutions at just one step in the strain rate below the point of flame extinction as defined in Table 2. As this step size is less than 3% of the value of the global strain rate, this should be the upper bound on the computed error in the local strain rate at the actual point of extinction.

Predicted values of the local near extinction strain rate and global strain rate at extinction are compared in Figure 7, where the results for the syngas compositions and syngas–methane blends are shown in Figure 7(a) and (b), respectively, for both parabolic and uniform burner configurations. In the case of the parabolic burner configuration, the predictions of global and local strain rates are generally in good agreement for a wide range of fuel compositions, dilution mole fractions, and flow rates. Some notable differences include a slight underestimation of the local strain rate by the global strain rate for low flow rates and the reversal of this trend as the global strain rate exceeds $a_g \approx 600\ s^{-1}$. As should be expected, the numerical results for the uniform inflow burner configuration have virtually identical values of the local strain rate near extinction when compared to the parabolic results. This supports the argument that the local near extinction strain rate is a fundamental property of the fuel mixture. However, the corresponding values of the global strain rates at extinction are now much higher and do not agree well with the parabolic inflow results. It would seem that the global extinction strain rate can be strongly dependent on the counter-flow flame flow field and nozzle inflow velocity distributions, should they deviate significantly from the ideal. These comparisons also suggest that the global strain rate at extinction for the parabolic burner configuration provides a more robust and superior estimate of local near extinction strain rate than that provided by the non-ideal uniform inflow configuration, at least for the present burner geometry and others like it considered in the literature.

## Nozzle exit-plane velocity profiles

While the importance of nozzle exit-plane inflow velocity distributions on flame extinction has been the subject of a few previous experimental studies (Korusoy and Whitelaw, 2001; Sarnacki et al., 2012) and very recently, Johnson et al. (2015) have performed an investigation of multi-dimensional effects in counter-flow burners and assessed requirements for the validity of quasi-1D theory, there have been still only a few previous multi-dimensional, high-fidelity, numerical studies of extinction of counter-flow diffusion flames. The 2D axisymmetric numerical solution method used here allows the detailed examination of the flow field within the entire solution domain and hence a study of the inflow velocity profiles at the exit plane of the nozzles as a function of the strain rate. The predicted normalized axial velocity profiles of the counter-flow diffusion flames for the

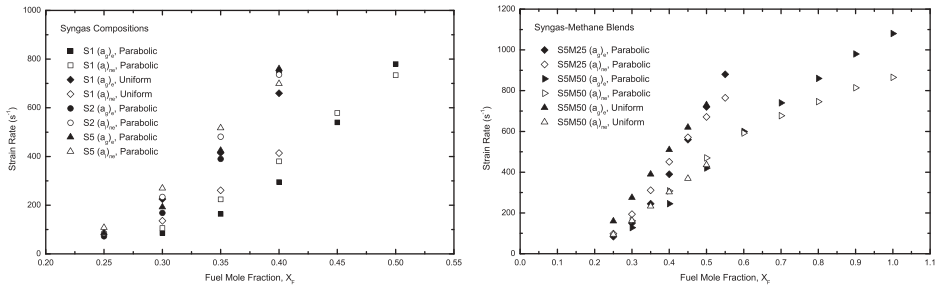


(a) Syngas compositions S1, S2, and S5.

(b) Syngas-methane blends S5M25 and S5M50X.

**Figure 7.** Comparison of predicted local extinction strain rates (white symbol) and global extinction strain rates (black symbol) for (a) three syngas compositions and (b) two syngas–methane blends.

syngas-methane blend S5M50 are given in Figure 8 for both the parabolic and uniform inflow burner configurations. Numerical results are given for several increasing strain rates. The idealized uniform and parabolic velocity profiles are also shown in the figure for comparison. For the parabolic inflow configuration at low strain rates, the velocity distribution at the nozzle exit plane closely resembles the ideal parabolic profile. However, as the strain rate increases, the peak at the center line is reduced and a more flat top distribution results. Further increases in strain rate lead to an exit plane velocity distribution with a depression near the nozzle center line with velocity maximums now occurring at locations away from the center line. These results suggest that the velocity distributions at the nozzle exit planes evolve from a nearly idealized parabolic profile to something that is very far from this as the flow rate increases and that this change is due to the influence of pressure gradients created by the interactions of the opposed-jet flow field and the presence of the flame. Sarnacki et al. (2012) have observed similar nozzle exit flow behavior in their experimental studies of opposed-jet flames.

The decrease in the axial center-line velocity with respect to the bulk flow velocity as strain rate increases can explain the apparent increase in the global strain rate relative to the local strain rate with increasing flow rate as observed previously in Figure 7 for the parabolic inflow cases. Furthermore, as the depression in axial velocity profiles at the nozzle exit plane becomes more significant with increasing flow rates (i.e., above $a_g \approx 600\ s^{-1}$), inspection of the numerical flame structure reveals that flame extinction no longer occurs at the center line, but takes place at some distance away from the center line where local maxima in the velocity profile results in elevated strain rates. In these cases, estimates of the local strain rate base on the velocity variation along the axial center line as computed here are no longer representative of the true local strain rate at extinction and in fact can result in the under-prediction of this value.

In contrast to the results for the parabolic inflow burner configuration, the nozzle exit-plane inflow velocity profiles for the uniform inflow configuration are more consistent across flow rates. While deviating from an ideal uniform, all of the profiles of Figure 8(b)

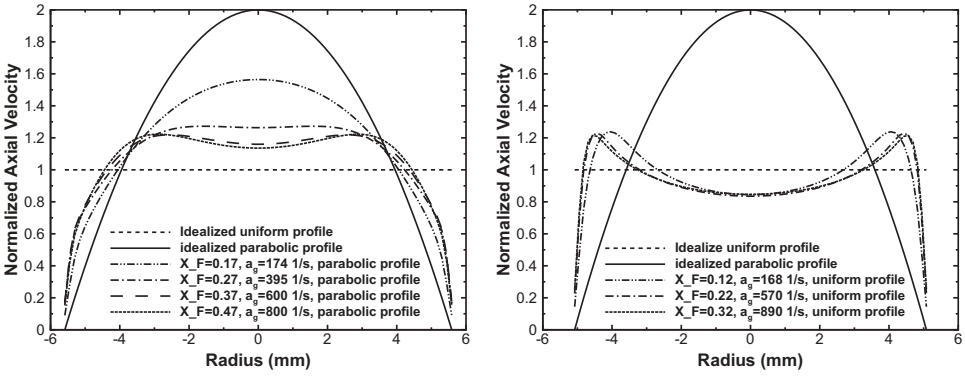


(a) Parabolic profile burner. (b) Uniform profile burner.

**Figure 8.** Comparison of predicted normalized air nozzle exit-plane inflow velocity profiles for various dilution fractions and global strain rates obtained for (a) parabolic and (b) uniform profile burner configurations with the syngas–methane blend S5M50 fuel.

exhibit a center-line dip in the velocity to about 84% of the bulk velocity and have peak values near the outer rim of the nozzle with a magnitude of about 122%. This consistency in the numerical results is caused by the enforcement of ideal uniform inflow velocity profile just 5.1 mm upstream of the nozzle exit plane at the location of the sintered metal matrix. Nevertheless, it is very doubtful that the matrix is capable of producing such a uniform flow profile in the actual experiments, particularly for elevated flow conditions. The deviation of actual experimental inflow distribution from the prescribed numerical inflow profile can serve as explanation for the somewhat poor and often under-prediction of global strain rate extinction values shown previously in Figure 5. Furthermore, the results of Figure 8 show that, at sufficiently high flow rates, the inflow velocity profile of the parabolic configurations starts to resemble that of the uniform case and this explains the decreasing differences in the global extinction strain rates for the two nozzle configurations as depicted in Figure 5(a) as the flow rates increase.

## Conclusions

A combined and systematic numerical and experimental study of extinction in counter-flow diffusion flames for syngas and syngas–methane blends was conducted. The high-fidelity 2D finite-volume scheme employed in the study was shown to provide good predictions of the counter-flow diffusion flame structure and to be capable of providing good estimates of the extinction strain that agree, both qualitatively and quantitatively, with the measured experimental values for the three syngas compositions and two syngas–methane blends of interest here. It was also shown that, while the presence of hydrogen plays a significant role in the elevated extinction limits of the syngas fuels and blends, the presence of methane appears to have the opposite effect. Furthermore, it was observed that carbon monoxide concentrations of less than 50% by volume do not significantly inhibit the reactivity of the syngas mixtures with high hydrogen content, thus leading to the expected elevated extinction limits. The relationship between global and local strain rates was also explored numerically and the differences explained through deviations in the nozzle exit plane velocity flow distributions from that of the ideal.

## Funding

This work was supported by grants from the Ontario Research Fund Research Excellence (ORF-RE) Program and the Southern Ontario Smart Computing for Innovation Platform (SOSCIP) of the Province of Ontario. Computational resources for performing simulations reported in the paper were provided by the SOSCIP program as well as the SciNet High Performance Computing Consortium at the University of Toronto and Compute/Calcul Canada through funding from the Canada Foundation for Innovation (CFI) and the Province of Ontario, Canada.

## References

Amantini, G., Frank, J.H., Smooke, M.D., and Gomez, A. 2007. Computational and experimental study of steady axisymmetric non-premixed methane counterflow flames. *Combust. Theory Model.*, **11**, 47–72.

Biofuel.org.uk. 2010. *What is syngas*. http://biofuel.org.uk/what-is-syngas.html.

Charest, M.R.J., Groth, C.P.T., and Gülder, Ö.L. 2010. A computational framework for predicting laminar reactive flows with soot formation. *Combust. Theory Model.*, **14**(6), 793–825.

Charest, M.R.J., Groth, C.P.T., and Gülder, Ö.L. 2011a. Effects of gravity and pressure on laminar co-flow methane-air diffusion flames at pressures from 1 to 60 atmospheres. *Combust. Flame*, **158** (5), 860–875.

Charest, M.R.J., Groth, C.P.T., and Gülder, Ö.L. 2011b. Numerical study on the effects of pressure and gravity in laminar ethylene diffusion flames. *Combust. Flame*, **158**(10), 1933–1945.

Charest, M.R.J., Joo, H.I., Groth, C.P.T., and Gülder, Ö.L. 2011. Experimental and numerical study of soot formation in laminar ethylene diffusion flames at elevated pressures from 10 to 35 atm. *Proc. Combust. Inst.*, **33**, 549–557.

Ding, N., Arora, R., Norconk, M., and Lee, S.Y. 2011. Numerical investigation of diluent influence on flame extinction limits and emission characteristic of lean-premixed $H_2$-CO (syngas) flames. *Int. J. Hydrogen Energy*, **36**, 3222–3231.

Du, J., and Axelbaum, R.L. 1995. The effect of flame structure on soot-particle inception in diffusion flames. *Combust. Flame*, **100**, 367–375.

Egolfopoulos, F.N., Cho, P., and Law, C.K. 1989. Laminar flame speeds of methane-air mixtures under reduced and elevated pressures. *Combust. Flame*, **76**, 375–391.

Fleck, J.M., Griebel, P., Steinberg, A.M., Arndt, C.M., and Aigner, M. 2013. Auto-ignition and flame stabilization of hydrogen/natural gas/nitrogen jets in a vitiated cross-flow at elevated pressure. *Int. J. Hydrogen Energy*, **38**(36), 16441–16452.

Gao, X., and Groth, C.P.T. 2006. A parallel adaptive mesh refinement algorithm for predicting turbulent non-premixed combusting flows. *Int. J. Comput. Fluid Dyn.*, **20**(5), 349–357.

Gao, X., Northrup, S.A., and Groth, C.P.T. 2011. Parallel solution-adaptive method for two-dimensional non-premixed combusting flows. *Prog. Comput. Fluid Dyn.*, **11**(2), 76–95.

Goodwin, D.G. 2003. An open-source, extensible software suite for CVD process simulation. *Chem. Vap. Deposition XVI EUROCVD*, **14**, 155–162.

Herzler, J., and Naumann, C. 2008. Shock tube study of the ignition of lean CO/$H_2$ fuel blends at intermediate temperatures and high pressure. *Combust. Sci. Tech.*, **180**(10–11), 2015–2028.

Johnson, R.F., VanDine, A.C., Esposito, G.L., and Chelliah, H.K. 2015. On the axisymmetric counterflow flame simulations: is there an optimal nozzle diameter and separation distance to apply quasi one-dimensional theory? *Combust. Sci. Tech.*, **187**, 37–59.

Kéromnès, A., Metcalfe, W.K., Heufer, K.A., Donohoe, N., Das, A.K., Sung, C.-J., … Curran, H.J. 2013. An experimental and detailed chemical kinetic modeling study of hydrogen and syngas mixture oxidation at elevated pressures. *Combust. Flame*, **160**(6), 995–1011.

Korusoy, E., and Whitelaw, J.H. 2001. Opposed jets with small separations and their implications for the extinction of opposed flames. *Exp. Fluids*, **31**, 111–117.

Mittal, G., Sung, C.J., Fairweather, M., Tomlin, A.S., Griffiths, J.F., and Hughes, K.J. 2007. Significance of the $HO_2$ + CO reaction during the combustion of CO + $H_2$ mixtures at high pressures. *Proc. Combust. Inst.*, **31**(1), 419–427.

Park, J., Kim, J.S., Chung, J.O., Yun, J.H., and Keel, S.I. 2009. Chemical effects of added $CO_2$ on the extinction characteristics of $H_2$/CO/$CO_2$ syngas diffusion flames. *Int. J. Hydrogen Energy*, **34**, 8756–8762.

Pellett, G.L., Isaac, K.M., Humphreys, W.M., Gartrell, L.R., Roberts, W.L., Dancey, C.L., and Northam, G.B. 1998. Velocity and thermal structure, and strain-induced extinction of 14 to 100% hydrogen-air counterflow diffusion flames. *Combust. Flame*, **112**, 575–592.

Roe, P.L. 1981. Approximate Riemann solvers, parameter vectors, and difference schemes. *J. Comput. Phys.*, **43**, 357–372.

Sachdev, J.S., Groth, C.P.T., and Gottlieb, J.J. 2005. A parallel solution-adaptive scheme for predicting multi-phase core flows in solid propellant rocket motors. *Int. J. Comput. Fluid Dyn.*, **19**(2), 159–177.

Sarnacki, B.G., Esposito, G., Krauss, R.H., and Chelliah, H.K. 2012. Extinction limits and associated uncertainties of nonpremixed counterflow flames of methane, ethylene, propylene and n-butane in air. *Combust. Flame*, **159**, 1026–1043.

Seshadri, K., and Williams, F.A. 1978. Laminar flow between parallel plates with injection of a reactant at high reynolds number. *Int. J. Heat Mass Trans.*, **21**, 251–253.

Shih, H.Y., and Hsu, J.R. 2011. A computational study of combustion and extinction of opposed-jet syngas diffusion flames. *Int. J. Hydrogen Energy*, **36**, 15868–15879.

Slavinskaya, N., Braun-Unkhoff, M., and Frank, P. 2008. Reduced reaction mechanisms for methane and syngas combustion in gas turbines. *J. Engin. Gas Turbines Power*, **130**, 1–6.

Smith, G.P., Golden, D.M., Frenklach, M., Moriarty, N.W., Eiteneer, B., Goldenberg, M., … Qin, Z. 2000. *GRI-Mech 3.0*. http://www.me.berkeley.edu/grimech/.

Som, S., Ramirez, A.I., Hagerdorn, J., Saveliev, A., and Aggarwal, S.K. 2008. A numerical and experimental study of counterflow syngas flames at different pressures. *Fuel*, **87**, 319–334.

Somerville, C., Youngs, H., Taylor, C., Davis, S.C., and Long, S.P. 2010. Feedstocks for lignocellulosic biofuels. *Science*, **329**, 790–792.

Thiessen, S., Khalil, E., and Karim, G. 2010. The autoignition in air of some binary fuel mixtures containing hydrogen. *Int. J. Hydrogen Energy*, **35**(18), 10013–10017.

Vagelopoulos, C.M., and Egolfopoulos, F.N. 1998. Direct experimental determination of laminar flame speeds. *Proc. Combust. Inst.*, **27**, 513–519.

Wang, W. 2014. *Experimental and numerical investigation of structure and extinction limits of biofuels in laminar counterflow diffusion flames* (Unpublished master's thesis). University of Toronto.

Weiss, J.M., and Smith, W.A. 1995. Preconditioning applied to variable and constant density flows. *Aiaa J.*, **33**(11), 2050–2057.

Williams, B.A. 2001. Sensitivity of calculated extinction strain rate to molecular formulation in nonpremixed counterflow flames. *Combust. Flame*, **124**, 330–333.

Xia, F., and Axelbaum, R.L. 2013. Simplifying the complexity of diffusion flames through interpretation in C/O ratio space. *Comp. Math. Applic.*, **65**(10), 1625–1632.

Yu, G., Law, C.K., and Wu, C.K. 1986. Laminar flame speeds of hydrocarbon + air mixtures with hydrogen addition. *Combust. Flame*, **63**, 339–347.